Journal Pre-proof

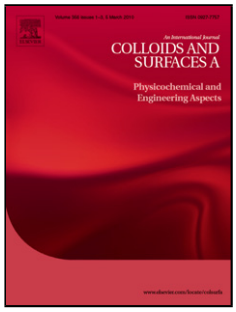

A fundamental study of adsorption kinetics of surfactants onto metal oxides using quartz crystal microbalance with dissipation (QCM-D)

Sandra C. Medina (Conceptualization) (Methodology) (Data curation) (Investigation) (Formal analysis) (Project administration)<ce:contributor-role>Writing - Original draft), Andreia S.F. Farinha (Methodology) (Formal analysis)<ce:contributor-role>Writing - Original draft), Abdul-Hamid Emwas (Data curation) (Formal analysis), Assiyeh Tabatabai (Conceptualization) (Formal analysis) (Writing - review and editing) (Supervision), TorOve Leiknes (Writing - review and editing) (Supervision) (Funding acquisition)

PII: S0927-7757(19)31232-4

DOI: https://doi.org/10.1016/j.colsurfa.2019.124237

Reference: COLSUA 124237

To appear in: *Colloids and Surfaces A: Physicochemical and Engineering Aspects*

Received Date: 15 September 2019

Revised Date: 14 November 2019

Accepted Date: 15 November 2019

Please cite this article as: Medina SC, Farinha ASF, Emwas A-Hamid, Tabatabai A, Leiknes T, A fundamental study of adsorption kinetics of surfactants onto metal oxides using quartz crystal microbalance with dissipation (QCM-D), *Colloids and Surfaces A: Physicochemical and Engineering Aspects* (2019), doi: https://doi.org/10.1016/j.colsurfa.2019.124237

A fundamental study of adsorption kinetics of surfactants onto metal oxides using quartz crystal microbalance with dissipation (QCM-D)

*Sandra C. Medina[*a], Andreia S. F. Farinha[a], Abdul-Hamid Emwas[b], Assiyeh Tabatabai[a,c], TorOve Leiknes [a]*

[a] Water Desalination and Reuse Center (WDRC), King Abdullah University of Science and Technology (KAUST), Thuwal 23955-6900, Saudi Arabia.

[b] Imaging and Characterization Core Lab, King Abdullah University of Science and Technology (KAUST), Thuwal 23955-6900, Saudi Arabia.

[c] /KRLVW%XVLQHVV,QQRYDWLRQ&HQWHU5XHGH1400 Nivelles, Belgium.

Abbreviations: QCM-D, quartz crystal microbalance with dissipation; PW, Produced Water; SDBS, Sodium Dodecyl Benzene Sulphonate; CTAB, cetyltrimethylammonium bromide; CMC, critical micelle concentration; NMR, nuclear magnetic resonance.

*Corresponding author: Sandra C. Medina. e-mail: sandra.medina@kaust.edu.sa. 4700 King Abdullah University of Science and Technology (KAUST) Thuwal, 23955-6900, Saudi Arabia. Tel: +966545754908.

E-mail addresses: sandra.medina@kaust.edu.sa (S.C. Medina), andreia.farinha@kaust.edu.sa (A.S.F. Farinha), abdelhamid.emwas@kaust.edu.sa (A.H. Emwas), assiyeh.tabatabai@gmail.com (A. Tabatabai), torove.leiknes@kaust.edu.sa (T. Leiknes)

Graphical Abstract

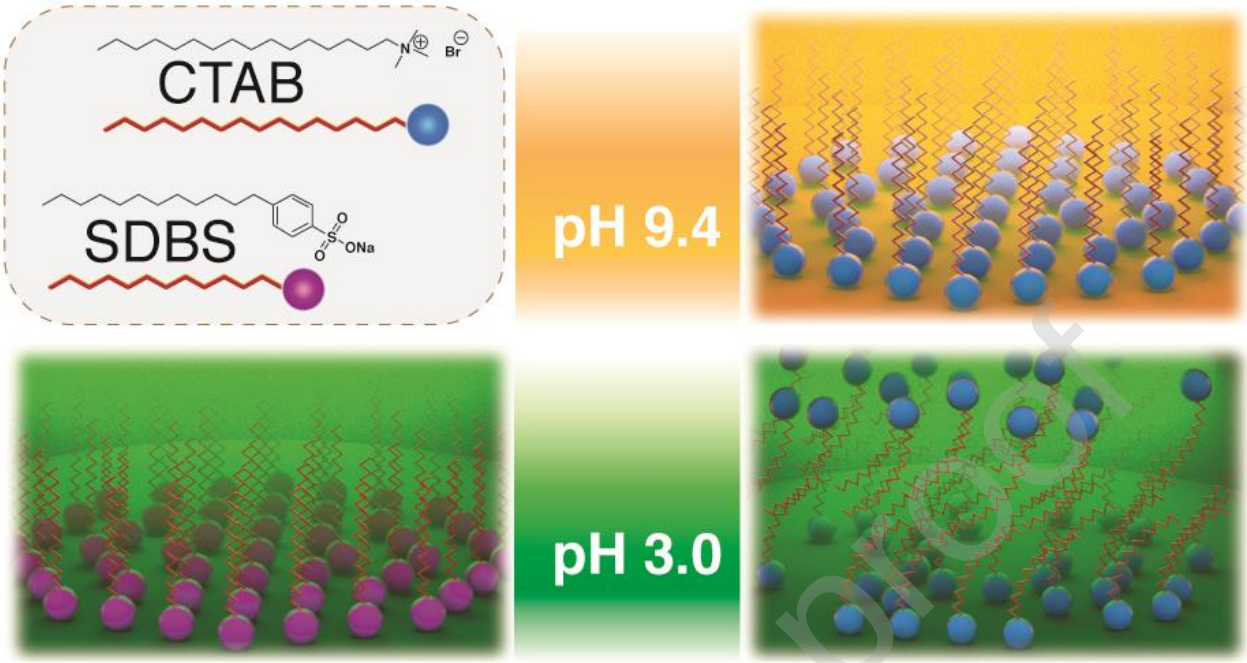

ABSTRACT

Hypothesis

Membrane fouling challenges the viability of oil-field produced water (PW) treatment with ceramic membranes. Surfactants play an important role in irreversible fouling through adsorption phenomena. However, previous studies have shown contradictory results. Hence, a fundamental understanding of surfactants-metal oxides interactions is necessary.

Experiments

In this work, we assessed the adsorption interactions of anionic SDBS and cationic CTAB with titania, zirconia and alumina surfaces, using the quartz crystal microbalance with dissipation (QCM-D) technique.

Findings

We found that electrostatic interactions controlled the adsorption of SDBS onto all the surfaces studied, with titania being the most likely to adsorb SDBS. On the contrary, CTAB was adsorbed regardless of the overall metal oxide surface charge. CTAB showed a two-step adsorption at acidic pH (3.0). In the first step, a rigid film was formed with a smaller adsorption capacity compared to the neutral (6.8) and basic (9.4) pH conditions. In the second step, a viscoelastic film was formed. Our results suggest that adsorption was driven by the nature of the surfactant rather than the metal oxide properties. This implies that electrostatic interactions should not be taken as the only predicting factor of adsorption phenomena in the understanding of PW fouling in ceramic membranes as other supramolecular interactions are strongly involved.

KEYWORDS: Surfactant adsorption, metal oxide, QCM-D, ceramic membrane, produced water.

INTRODUCTION

The application of ceramic membrane filtration in the treatment of oil-field produced water (PW) has been widely studied in recent years in an attempt to meet increasingly stringent regulations on discharge. These requirements stipulate that levels of emulsified and dissolved oil (*i.e.* oil droplets <10 m and <5 m, respectively (Weschenfelder et al., 2015c)) in PW discharge should not exceed 30 mg/L for all facilities in the Middle East, Malaysia, North Sea, Australia, Canada, Brazil, Ecuador, Colombia, etc. (Jiménez et al., 2018), or 5.0 mg/L for both oil and suspended solids for reinjection purposes (Weschenfelder et al., 2015b). Ceramic membranes have shown good performance in the treatment of oil/water emulsions in industrial applications with harsh operating conditions, i.e., high temperatures and aggressive chemicals (Weschenfelder et al., 2015a, Weschenfelder et al., 2015c). However, membrane fouling is a fundamental limitation for the economic viability of membrane treatment application in PW treatment (Lu et al., 2015). The mechanisms of membrane fouling by PW have not yet been fully described (Fouladitajar et al., 2013). However, fouling has been attributed to a combination of mechanisms including: (i) oil droplets coalescing and forming a layer on the membrane surface; (ii) oil droplets squeezing through the pores allowing partial permeation; (iii) adsorption of oil droplets and surfactants on the membrane surface and within the pores (Chakrabarty et al., 2008, Silalahi et al., 2009, Ebrahimi et al., 2010, Matos et al., 2016, Tummons et al., 2016). Furthermore, these mechanisms may be occurring simultaneously, making the study of membrane fouling more complex (Iritani et al., 2014). To improve understanding of membrane fouling mechanisms during PW treatment, each phenomenon should be studied and understood separately.

Surfactants present in oil/water emulsions have been shown to play a key role in irreversible fouling development during ceramic membrane filtration (Faibish and Cohen, 2001, Fernández et al., 2005, Lu et al., 2015). Surfactant molecules directly affect the emulsion stability through their interactions with the membrane surface and pores (Faibish and Cohen, 2001). Various chemicals added at different stages of crude oil production also have surface-active properties. For instance, chemicals used for oil recovery, crude

oil dehydration, biological control, corrosion inhibition and extraction enhancement can act as surfactants, ending up in the PW once the crude oil has been separated. Surfactant molecules contain hydrophilic and hydrophobic moieties, which are adsorbed at the oil/water interface and significantly decrease the interfacial surface tension by significant amount • mN/m) when present at low concentrations, *i.e.,* ” 0.01 M (Seyed Shahabadi and Reyhani, 2014). As the concentration of a surfactant increases in solution, the monomers agglomerate and self-assemble in micelles. These micelles start to form within a very narrow concentration range known as the FULWLFDOPLFHOOHFRQFHQWUDWLRQ&0&, where they coexist in equilibrium with surfactant monomers. A study by Dickhout et al. (2017) showed that micelles that form above the CMC are retained by UF membranes because their diameters are comparable to UF membrane pore sizes (*i.e.*, 1-10 nm), while surfactant monomers tend to adsorb onto the membrane surface due to electrostatic forces or hydrophobic/hydrophilic interactions. These factors affect membrane surface characteristics, leading to changes in permeate flux and solute rejection. The degree of adsorption depends on the surfactant type and membrane material properties (Berg, 2010).

Previous studies have reported that electrostatic-based correlations between the membrane surface charge and the surfactant charge in oil/water emulsions can prevent ceramic membrane fouling. However, reported results are contradictory, suggesting that electrostatic interactions do not fully explain membrane fouling. For example, Matos et al. (2016) found an increase in UF permeate flux when the membrane surface (zirconia / titania) and emulsion droplets (at pH 6.5-7.5) had the same charge, and a decrease in UF permeate flux when they had opposite charges. In contrast, Lu et al. (2016) suggested using a metal oxide with a surface charge opposite to that of the emulsion in order to alleviate irreversible membrane fouling. However, there is wide variability in these experiments and a clear background understanding of the interaction of surfactants with metal oxides is required.

The aim of this study is to clarify the state of the art by assessing the effect of adsorption rates and interactions of charged surfactants with commonly used ceramic membrane materials, utilizing the quartz crystal microbalance with dissipation (QCM-D) technique. QCM-D is a sensitive analytical instrument

based on piezoelectric AT-cut quartz crystal and gold electrodes, which allows real-time detection of structural and mass changes of the material being adsorbed/desorbed onto the sensor (Dixon, 2008). In membrane fouling studies, investigation of surfactant adsorption with QCM-D has been reported previously for polymeric materials (e.g., PES (Liu and Kim (2009)) and PVDF/SiO_2-PNIPAM (Ngang et al. (2017))). However, to our knowledge no studies have yet been carried out for adsorption on ceramic membrane materials. In this study, the adsorption kinetics of two charged surfactants (SDBS (anionic) and CTAB (cationic)) onto titania, zirconia and alumina surfaces were investigated. In addition, the effect of pH on adsorption rates and capacity of surfactant solutions on the metal oxides were investigated.

MATERIALS AND METHODS

Materials

Two surfactants, sodium dodecylbenzene sulfonate (SDBS), MW 343.4 g/mol, pKa 2.2, CMC ~2.0 mM (Hait et al., 2003)) and cetyltrimethylammonium bromide (CTAB), MW 364.4 g/mol pKa 9.5, CMC ~0.8 mM (Moulik et al., 1996)) were purchased from Sigma-Aldrich and used as received.

Surfactant solutions were prepared by dissolving specified amounts in Milli-Q water (resistivity of 18.2). pH adjustment was achieved by adding 0.1 M solutions of sodium hydroxide or sulfuric acid. The formation of suspended crystals of CTAB was observed DW VXUIDFWDQW FRQFHQWUDWLRQV •P0 7KHVH crystals were formed due to the Krafft point of CTAB (between 20-25 °C 0DQRMORYLü), corresponding to the temperature range in which the solutions were prepared. For higher concentration samples, a sonication step of 10 min was carried out.

Three metal oxide sensors were used in the QCM-D adsorption studies, titania, zirconia and alumina (Biolin Scientific AB, Sweden). QCM-D sensors surfaces were selected as the system allows the study on the metal oxide/surfactant interaction itself, controlling the experimental conditions and avoiding the hydrodynamic effects on the adsorption. This is possible due to the low roughness at the sensor surface

(below 2nm, according to manufacturer specifications) and the laminar flow regime within the sensor chamber (e.g., at 150 L/min inflow) (Kwon et al., 2009). The fluid-dynamic effect on the transport limitation of the adsorption was not addressed in this particular work. However, QCM-D allows the comparation of kinetics in specific experimental conditions (Gutig et al., 2008). The characteristics of coated QCM-D sensors are assumed to behave in a similar fashion in the nanoscale as a ceramic membrane surface. In the actual ceramic membrane, adsorption interaction might be further exaggerated as result of more are available contact area (i.e., membrane porosity and roughness) and hydrodynamic forces such as permeation drag. For sensor cleaning, UV/Ozone ProCleaner^{TM}220 (Bioforce Nanosciences Inc., USA) and Hellmanex® III (Hellma Analytics, Germany) were used.

QCM-D data acquisition and processing

QCM-D analysis was performed with a Q-Sense analyzer (Biolin Scientific AB, Sweden). Both resonance frequency (F) and energy dissipation (D) were recorded from the different overtones. Surfactant adsorption on the oxide surface induces variation in frequency and dissipation (û*F* and û*D*). Frequency variation (û*F*) is proportional to the adsorbed mass (ûm) and in the case of rigid films, can be determined by the Sauerbrey equation (1),

$$¿ \bullet \quad L\ F\ \frac{¿}{\bullet} : s ;$$

Where, ûm is the mass variation per area of the sensor (ng/cm^2), û*F* is the variation of frequency (Hz), C is a constant (17.8 ng/cm^{2}Hz) and n is the harmonic number (« 13).

For soft films, where there is a large change in û*D* (*i.e.*, > ~1x10^{-6}), the linearity between ûF and û*m* in the Sauerbrey relation is no longer valid (Kou and Xu, 2016). In this case, the one-layer Voigh viscoelastic model was applied utilizing the software QTools (Biolin Scientific AB, Sweden). The model assumes a homogeneous thickness, density and no-slip conditions of the adsorbed film. The Voigh model back-calculates the viscoelastic properties of a film (*i.e.*, elasticity, viscosity, thickness and mass) with the

measured û*D* and û*F* in different overtones (Reviakine et al., 2011). The measurements from overtones 9, 11 and 13 were used as input for the soft film modeling as they showed lower noise.

The cleaning procedure of the quartz sensors was found to be critical for ensuring reproducibility of results. Sensor cleaning was performed by submerging the sensor in a 1% (v/v) solution of Hellmanex® III for 30 min, followed by rinsing with deionized water and drying with a clean nitrogen gas stream. Thereafter, the sensor was sonicated for 10 min in ethanol before UV/Ozone treatment for 10 min. Sensors were reused a maximum of five times following this procedure.

Prior to each measurement of adsorption kinetics, a baseline was obtained by rinsing the sensor with Milli-Q water at a constant rate of 150 L/min. The baseline should not drift by more than 0.5 Hz for at least 1 h to ensure stability and reliability of the experiment (Lu et al., 2016). Thereafter, the surfactant solution was fed into a controlled QCM-D chamber temperature at 22 °C. Measurements were performed in duplicate.

Kinetics Models

Real-time acquisition of frequency variations over time (t), induced by surfactant adsorption/accumulation on the oxide surface provided the basis for the kinetics studies. Experimental data was fitted using pseudo-first order (2) and pseudo-second order equations (3) (Kou and Xu, 2016).

$$MHL\ MAs\ F\ A^{?}\ -ç;) \quad (2)$$

$$MHL\ \frac{.\ çä Ð.}{5>ä Ð\ .\ ç} \quad (3)$$

Where qt and qe are the amount of surfactant adsorbed at time t and at equilibrium, respectively, expressed in mass per unit area (ng/cm^2). $_1$ and $_2$ are apparent rate constants of pseudo-first-order (1/s) and pseudo-second order (cm^2/ng.s), respectively. The fitting model with the lowest root mean square error, as described by Largitte and Pasquier (2016), was defined as the best model for the system.

The adsorption kinetics of surfactant S and metal oxide M is described in equation (4) as a reversible system with adsorption rate *k*, desorption rate k^{-1} and an overall rate of k/k^{-1}.

$$5\ E\ /\ \frac{\dot{O}}{\dot{O}^{\prime}}\ 5/ \quad (4)$$

k and k^{-1} rates are calculated from the linear correlation of the apparent rate $_{1,2}$ with surfactant concentration as is shown in equation (5).

$$\acute{U}_{5\&} L\ \ GH\,\%E\ G^{?}\,5 \quad (5)$$

Where *k* (slope) and k^{-1} (y-intercept) are expressed in units of 1/s.mM and 1/s, respectively for pseudo-first order and in cm^2/mM.ng.s and cm^2/ng.s for pseudo second order kinetic models.

RESULTS AND DISCUSSION

The interactions of SDBS and CTAB with three metal oxide surfaces were studied in terms of kinetics of adsorption at pH 6.8. For all SDBS and CTAB concentrations, the frequency plateau was reached in less than 2 h. The adsorption of both SDBS and CTAB on the tested metal oxides resulted in the formation of rigid films at pH 6.8, as û*D* values were lower than $1x10^{-6}$ (û*D* max. of $0.3x10^{-6}$) and û*F* in the different overtones overlapped. The Sauerbrey equation was therefore used to obtain ûm, where the average frequency variation of overtones 7, 9 and 11 were used, as they showed lower noise (example in Figure S1a), in agreement with (Kou and Xu, 2016). The results were then analyzed and fitted with pseudo-first and pseudo-second order equations (Eq. 2 and Eq. 3). The experimental data was found to be best described by a pseudo-second order fit (example in Figure S1b).

Adsorption kinetics of SDBS

Calculated values of the apparent rate constant ($_2$) and the amount of SDBS surfactant adsorbed (qe) for the pseudo-second order kinetic model are presented in Figure 1 and summarized in Table S1 of the

Supplementary material. The results of adsorption at low concentrations of SDBS are not shown as the frequency drift was found to be in range with system noise (i.e., 0.3 Hz).

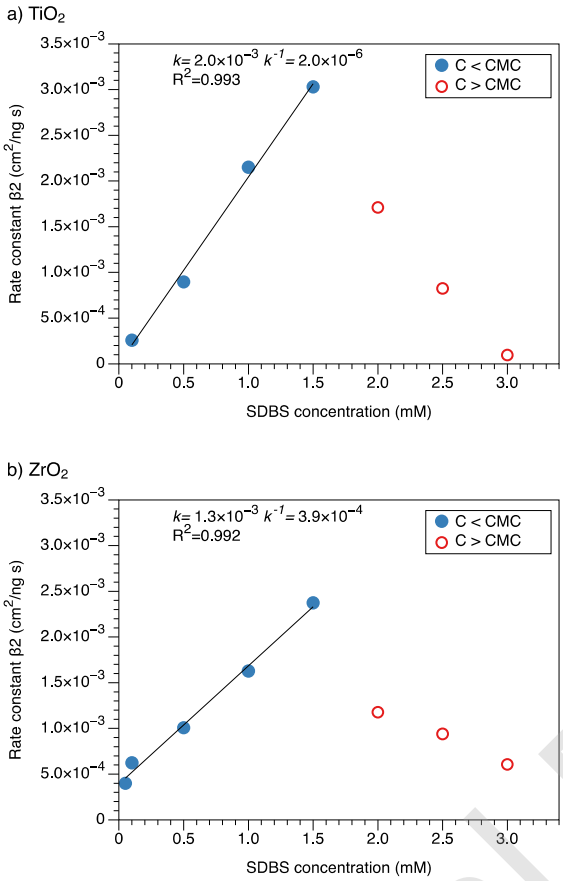

Figure 1. Apparent rate of adsorption $_2$ (left side graphs) and amount of SDBS adsorbed qe (right side graphs) for the systems a) titania; b) zirconia; and c) alumina at pH 6.8

A linear increase in $_2$ for increasing concentrations of SDBS was observed for all metal oxides before reaching the CMC of 2 mM (Figure 1). At concentrations equal to or greater than the CMC, $_2$ values no longer followed the same linear behavior. $_2$ decreased abruptly for titania (Figure 1a) and zirconia (Figure 1b), whereas no discernible trend was observed for alumina (Figure 1c). This suggests that the aggregation of SDBS molecules in spherical shaped micelles (*i.e.*, aggregation number of 57 (Sood and Aggarwal, 2018)) result in slower adsorption kinetics due to the presence of repulsive intermicellar interactions (Cheng and Gulari, 1982). However, the intermicellar repulsive interactions were not strong enough to prevent further SDBS adsorption onto the metal oxides, because the adsorption capacity qe continued to increase at higher concentrations.

The rate of adsorption k (slope) and desorption k^{-1} (y-intercept) were calculated from the linear dependence of $_2$ on surfactant concentration (Eq. 5) in Figure 1 and are summarized in Table 1. The ratios k/k^{-1} were determined to understand the overall adsorption reaction. At higher k/k^{-1} ratios, the overall system was more delocalized to surfactant adsorption. SDBS was observed to have similar adsorption rates (k) for titania and zirconia. However, the desorption rate of titania (k^{-1}= 2.0x10^{-5} cm^2/ng.s) was one order of magnitude lower than that of zirconia (k^{-1} = 3.9x10^{-4} cm^2/ng.s). Therefore, the overall adsorption k/k^{-1} ratio of SDBS on titania (1000.0 1/mM) was the highest. This indicates that the fouling potential of SDBS is higher for ceramic membranes based on titania as compared with zirconia or alumina. This is not related to the rate of adsorption but rather due to slower desorption rates.

For SDBS adsorption on alumina, the higher fluctuations in the linear relation of $_2$ with concentration observed in Figure 1c (R^2=0.910) may be explained by a less organized adsorption. The adsorption rate (k = 2.7x10^{-4} cm^2/mM ng.s) is of the same order of magnitude as the desorption rate (k^{-1}= 6.6x10^{-4} cm^2/ng.s), resulting in the smallest k/k^{-1} ratio (0.4 1/mM). These findings support the choice of alumina material over the other metal oxides, been alumina the most common material used in ceramic membranes (Saad Alami et al., 2018).

To evaluate the effect of the metal oxide surface charge on adsorption kinetics experiments were conducted at pH values above and below the zero-point charge (pH_{pzc}) of the metal oxides. According to data summarized by Kosmulski (2006), pH_{pzc} ranges between 5.2-6.3 for titania, 5.5-6.6 for zirconia and 7.4-8.6 for alumina. These values were taken from literature as the sensors are coated with high purity metal oxides equivalent to the pure state of the material. In this study, adsorption kinetics were obtained at pH values of 3.0 and 9.4, for 1 mM SDBS concentration. The results were fitted using the pseudo-second order model as above, with calculated parameters summarized in Table 2. Values of adsorption kinetics at pH 6.8 are included in this table for comparison.

Adsorption rates ($_2$) under acidic conditions (pH 3.0) were slower for the three metal oxides in comparison to the values calculated for pH 6.8 and 9.4. This was especially evident for SDBS-titania where $_2$ at pH 3.0 ($3.3x10^{-7}$ $cm^2/ng.s$) was four orders of magnitude lower than the values obtained at higher pH ($2.2x10^{-3}$ at pH 6.8, $2.1x10^{-3}$ $cm^2/ng.s$ at pH 9.4). Slower adsorption rates under acidic conditions can be related to the formation of SDBS micelles on the metal oxide surfaces as a result of the accumulation of molecules, as evidenced by the high adsorption capacities qe (e.g., 569.8 ng/cm^2 SDBS on titania at pH 3.0). The presence of SDBS micelles on the surfaces of the three metal oxides under acidic conditions was confirmed by the QCM-D dissipation ($\hat{u}D$) values, which were close to but still under the threshold (*i.e.*, $1x10^{-6}$) at which the adsorbed films could be considered viscoelastic (Kou and Xu, 2016). In general, relatively high $\hat{u}D$ of $0.3x10^{-6} \pm 0.6x10^{-6}$ were obtained at pH 3.0 compared to $0.01x10^{-6} \pm 0.1x10^{-6}$ at higher pH. QCM-D results of $\hat{u}D$ and $\hat{u}F$ for the SDBS adsorption on the three metal oxides at different pH are shown in Figure S3.

Although adsorption rates were lower under acidic conditions, the capacity of SDBS adsorption (qe) onto all metal oxides surfaces was highest at pH 3.0, decreasing with increasing pH. This can be attributed to changes in the overall surface charge of the metal oxides and the interactions with SDBS. At pH 3.0, the three metal oxides had an overall positive surface charge and the anionic characteristics of SDBS made it more likely to attach to the metal oxide surfaces, as evidenced by the higher qe values obtained. When the

pH was increased to 6.8, the surfaces of titania and zirconia tended towards a negative charge, while the surface charge for alumina was close to neutral. These shifts in surface charge caused a significant drop in qe values of 97.9% for titania, 90.8% for zirconia, and 84.8% for alumina. With a further increase of pH to 9.0, the qe continued to drop in smaller amounts (2.9%, 26.7% and 38.5% of the original values for pH 6.8) as the metal oxide surfaces became more negative, but no major surface charge shifts were observed. Furthermore, even with a negative overall charge on the metal oxide surfaces at pH 9.0, SDBS adsorption occurred at relatively fast rates (2.1x10-3 cm^2/ng.s on titania and alumina and 1.4x10-3 cm^2/ng.s on zirconia) and low qe (11.7, 18.2 and 17.9 ng/cm^2 for titania, zirconia and alumina, respectively). The occurrence of SDBS adsorption and reduced qe when the metal oxides carried a negative surface charge suggests the presence of positive sites of the surface even at basic conditions. These results reflect the important contribution of electrostatic interactions to the adsorption of anionic SDBS on the different metal oxides.

Adsorption kinetics of CTAB

Calculated values of the apparent rate constant ($_2$) and the amount of CTAB surfactant absorbed (qe) for the pseudo-second order equation (Eq 3) are summarized in Table S2, with corresponding graphical representation in Figure 2. For samples where the frequency variation was not negligible, a small signal-to-noise ratio was obtained (frequencies < 0.5 Hz, equivalent to 8.75 ng/cm^2). From the linear regression of $_2$, the calculated adsorption/desorption rate (k/k^{-1}) ratios of CTAB for the respective metal oxide systems are summarized in Table 3. No data is presented in Figure 2 or Table 3 for CTAB on alumina as the results indicated negligible adsorption under the conditions employed (û*F* results in Figure S3). These results are discussed later in this section.

Similar to the SDBS results, CTAB $_2$ rates on titania and zirconia showed a proportional relationship with increasing concentrations before reaching the CMC (0.8 mM). At the CMC, $_2$ abruptly declined to 2.1x10-5 cm^2/ng.s for titania but showed a higher qe of 397.4 ng/cm^2 (Figure 2a). In contrast, $_2$ for zirconia kept increasing to 3.4x10-5 cm^2/ng.s at the CMC (Figure 2b) but qe dropped to 175.2 ng/cm^2. These

differences in $_2$ and qe tendencies between titania and zirconia at the CMC can be explained by the formation of micelles on the metal oxide surfaces occurring at different concentrations. The agglomeration of CTAB molecules into spheroidal micelles (i.e., aggregation number of CTAB between 50 0DQRMORYLü 2012) and 66 3LViUDNHWDO) occurred faster on zirconia as it has a higher k/k^{-1} (13.8 1/mM in Table 3) than titania. At 0.6 mM CTAB, the highest qe value of 378.4 ng/cm^2 was reached on zirconia, however, when a higher concentration was applied (0.8 mM), repulsive intermicellar interactions (i.e., positive intermicellar interaction parameter of 0.025 1/mM (Javadian and Kakemam, 2017)) prevented further adsorption of the incoming micelles, and the qe decreased. On the other hand, due to the low k/k^{-1} ratio for titania (0.7 1/mM), the agglomeration of such quantities of CTAB molecules as required for micelle formation were not reached before the CMC, and only at the CMC was it possible to reach the highest qe of 397.4 ng/cm^2.

Both CTAB-titania and CTAB-zirconia systems presented comparable adsorption (k) rates (2.9x10^{-5} and 3.6x10^{-5} cm^2/mM ng.s, respectively). However, the desorption rate (k^{-1}) of zirconia (2.6x10^{-6} cm^2/ng.s) was one order of magnitude lower than that for titania (4.2x10^{-5} cm^2/ng.s). This gave a higher overall adsorption (k/k^{-1} value of 13.8 1/mM), indicating that CTAB is more likely to cause irreversible fouling in ceramic membranes based on zirconia due to the relatively low desorption rate.

Figure 2. Apparent rate of adsorption $_2$ (left side graphs) and amount of CTAB adsorbed qe (right side graphs) for the systems a) titania and b) zirconia at pH 6.8

The CTAB-alumina results indicated negligible adsorption. To confirm the lack of adsorption, an isotherm curve was obtained (Figure S4). An increase of CTAB concentrations did not lead to significant adsorption onto the alumina surface, suggesting that the charge distribution at the alumina surface is homogeneous, thus preventing CTAB from approaching the surface. The CTAB-alumina system was further investigated by FTIR-ATR. However, the resolution of the technique was too high to allow for any specific conclusion to be drawn (detailed information available in Text S1 and Figure S5). While literature on CTAB adsorption on alumina is scarce, our findings are in agreement with previous studies. The use of CTAB (at ambient pH ~7) has been studied in anti-corrosive composite coatings to prevent the attachment of alumina particles by repulsive electrostatic forces (Liu et al., 2009). In addition, in catalysis applications, hydroxycarboxylate derivatives have been utilized as linkers to attach CTAB on gamma alumina (Yue et al., 2010). Similarly to the adsorption results for SDBS at 6.8 pH condition, alumina content on ceramic membranes may have less impact on the formation of a CTAB fouling layer adsorbed onto the membrane surface.

To further understand the interactions of CTAB with the metal oxide surfaces, the rate of adsorption, $_2$, and qe were evaluated under acidic (pH 3.0) and basic (pH 9.4) conditions. Solutions of 0.6 mM CTAB

were chosen as this concentration is lower than the CMC, thus avoiding micelles formation, but high enough to be able to identify significant changes in ĵi during the first minutes of the run. The pseudo-second order kinetic model results are shown in Table 4. The $_2$ and qe values for pH 6.8 are included for comparison. The û*F* and û*D* results for the system CTAB-alumina at different pH values are shown in Figure 3.

Figure 3. QCM-D ûF and û*D* for CTAB 0.6 mM solution on a) titania, b) zirconia, and c) alumina at different pH values; d) two-step adsorption curve of 0.6 mM CTAB at pH 3.0 onto alumina, i) rigid film and ii) viscoelastic film formation.

Higher CTAB qe were obtained for all the metal oxides at basic pH conditions. This was expected as surfaces with overall negative charge might attract the positively charged CTAB. However, significant qe values were found for acidic CTAB solutions, with values equivalent to 87%, 78% and 49% of those

obtained under basic pH conditions for titania, zirconia and alumina, respectively. These findings suggest that electrostatic repulsion was not enough to prevent the surfactant adsorption under acidic conditions for all the metal oxides tested. Furthermore, the results of pH 3.0 clearly showed a two-step curve for all the systems (Figure 3d). The first step involved a relatively fast formation of a rigid film ($_2$ values of 6.38×10^{-5}, 1.2×10^{-4}, and 2.36×10^{-4} $cm^2/mM.ng.s$ for titania, zirconia and alumina, respectively), as confirmed by û values < 1×10^{-6} (Figure 3a, b and c). In the second step a viscoelastic film was formed, without reaching a plateau by the end of the run, and with û*D* values higher than 2×10^{-6}. The formation of this second layer indicates that CTAB was no longer organized in a rigid monolayer but in a viscoelastic bilayer. Thus, we propose that this new layer was sustained by hydrophobic interactions between surfactant tails, considering the excess of positive charges at the surface of the systems, as shown in Figure 3d.

The unexpected high qe value of 151.1 ng/cm^2 observed for the CTAB-alumina system at pH 3.0, compared to the negligible adsorption of CTAB-alumina at pH 9.8, was further investigated using solid-state proton NMR spectroscopy (^{1}H-NMR) to assess CTAB-alumina interactions at different pH values. ^{1}H-NMR analysis was performed as per the procedure described in Text S2. ^{1}H-NMR spectra results of alumina and CTAB-alumina at pH 3.0, 6.8, and 9.4 are shown in Figure 4.

Figure 4. 600MHz ^{1}H-NMR spectra of a) alumina b) alumina with CTAB adsorbed at pH 3.0, c) alumina with CTAB adsorbed at pH 6.8, and d) alumina with CTAB adsorbed at pH 9.4

The resonances generated by the protons of hydroxyl moieties at the alumina surface were observed around 1 ppm in all spectra obtained. No signals of the surfactant protons were observed at pH 6.8 (Figure 4c), confirming the absence of CTAB adsorption onto alumina at this pH. This is in agreement with results obtained from QCM-D analysis. Significant differences were found in the resonances due to the protons of CTAB tails at pH 3.0 and 9.4. At pH 3.0, well-defined signals appeared around 5 ppm (Figure 4b), while at pH 9.4, a broad signal was obtained at 6.98 ppm (Figure 4d). These signal differences suggest that the CTAB at pH 6.8 and 9.4 had been adsorbed onto alumina in a different mode. The narrower signals at pH 3.0 indicate that the molecular mobilities and dynamics of CTAB are higher than those at pH 9.4. These results are in agreement with the proposed model for the CTAB adsorption at pH 3.0 onto alumina, where a softer viscoelastic material is formed (Figure 3d). Moreover, the broadening of the signal at pH 9.4 as a

result of molecular rigidity provides more evidence of chemical shift anisotropy (CSA). CSA is usually the dominant broadening factor for ^{1}H-NMR spectra (Mroué et al., 2010). The observed downfield shift of the ^{1}H-NMR signal at pH 9.4 (*i.e.*, a signal at higher ppm) indicates that the surface is more prone to share electrons with the surfactant.

The possible effect of pH on pure alumina samples was also assessed by ^{1}H-NMR. These spectra are shown in Figure S6 of the Supplementary material. No significant differences were found in the alumina ^{1}H-NMR spectra at pH 3.0, 6.8 and 9.4, further confirming that adsorption is driven by the nature of the surfactant and not by the surface properties of the metal oxides.

CONCLUSIONS

The aim of this study was to gain a clear background understanding of surfactant adsorption phenomena onto commonly used ceramic membrane materials. QCM-D was successfully applied to obtain insights on SDBS and CTAB interactions with titania, zirconia and alumina surfaces. Adsorption of anionic SDBS onto the metal oxides resulted in the formation of a rigid film, where the positively charged surface adsorbed more surfactant because of electrostatic interactions. Compared to alumina and zirconia, titania was more readily saturated by SDBS, due to slower desorption processes. This implies that ceramic membranes based on titania in the composition will have higher fouling rates by SDBS adsorption due to slower desorption processes. Adsorption of cationic CTAB was based on complex interactions with the different metal oxide surfaces, where electrostatic repulsion did not prevent the adsorption of CTAB onto the positively charged metal oxide surfaces. CTAB was able to adsorb independently of the surface charge of the metal oxide and instead, the binding sites available between CTAB molecules and their interactions between surfactant tails seemed to play a major role. Alumina may be less readily fouled by CTAB compared to zirconia and titania, especially at neutral pH where negligible adsorption was found.

Alumina content on ceramic membranes may have less impact on the formation of a surfactant fouling layer adsorbed onto the membrane surface (regardless of SDBS or CTAB). These findings support the choice of alumina material over the other metal oxides, been alumina the most common material used in ceramic membranes.

QCM-D is a very sensitive method that can detect changes in mass at very low amounts. This allowed us to study the adsorption behavior / phenomena of charged surfactants and ceramic membrane materials typically used in PW treatment from a fundamental perspective and to distinguish between mechanisms governing the interactions under different conditions of pH / surfactant concentration. Our research showed in a quantitative manner using a straight forward approach with a highly sensitive method, that the choice of surfactant is more critical than the membrane material in fouling considerations in produced water treatment applications. The adsorption interactions are commanded by the nature and properties of the surfactant rather than the metal oxide properties. This has implications in the understanding of fouling mechanisms of produced water in ceramic membranes. Electrostatic interactions should not be taken as the only predicting factor of adsorption phenomena as other supramolecular interactions are strongly involved. The choice of chemicals for upstream oil & gas production can have a significant impact on the performance and recovery of ceramic membrane systems applied for PW treatment. Further research is required on cleaning strategies for ceramic membrane materials fouled by different surfactants.

ACKNOWLEDGMENTS

The research reported in this publication was supported by funding from King Abdullah University of Science and Technology (KAUST).

The authors are grateful for the input from Asst. Prof. Dr. Himanshu Mishra and Dr. Adriano Santana from Water Desalination and Reuse Center at KAUST.

The abstract art and Figure 3d were created by Heno Hwang, scientific illustrator at KAUST.

REFERENCES

BERG, J. C. 2010. Thermodynamics of Interfacial Systems. *An Introduction to Interfaces and Colloids: The Bridge to Nanoscience.* World Scientific Publishing Co. Pte. Ltd.

CHAKRABARTY, B., GHOSHAL, A. K. & PURKAIT, M. K. 2008. Ultrafiltration of stable oil-in-water emulsion by polysulfone membrane. *Journal of Membrane Science,* 325**,** 427-437.

CHENG, D. C. H. & GULARI, E. 1982. Micellization and intermicellar interactions in aqueous sodium dodecyl benzene sulfonate solutions. *Journal of Colloid and Interface Science,* 90**,** 410-423.

DICKHOUT, J. M., MORENO, J., BIESHEUVEL, P. M., BOELS, L., LAMMERTINK, R. G. H. & DE VOS, W. M. 2017. Produced water treatment by membranes: A review from a colloidal perspective. *Journal of Colloid and Interface Science,* 487**,** 523-534.

DIXON, M. C. 2008. Quartz crystal microbalance with dissipation monitoring: enabling real-time characterization of biological materials and their interactions. *Journal of biomolecular techniques : JBT,* 19**,** 151-158.

EBRAHIMI, M., WILLERSHAUSEN, D., ASHAGHI, K. S., ENGEL, L., PLACIDO, L., MUND, P., BOLDUAN, P. & CZERMAK, P. 2010. Investigations on the use of different ceramic membranes for efficient oil-field produced water treatment. *Desalination,* 250**,** 991-996.

FAIBISH, R. S. & COHEN, Y. 2001. Fouling and rejection behavior of ceramic and polymer-modified ceramic membranes for ultrafiltration of oil-in-water emulsions and microemulsions. *Colloids and Surfaces A: Physicochemical and Engineering Aspects,* 191**,** 27-40.

FERNÁNDEZ, E., BENITO, J. M., PAZOS, C. & COCA, J. 2005. Ceramic membrane ultrafiltration of anionic and nonionic surfactant solutions. *Journal of Membrane Science,* 246**,** 1-6.

FOULADITAJAR, A., ZOKAEE ASHTIANI, F., OKHOVAT, A. & DABIR, B. 2013. Membrane fouling in microfiltration of oil-in-water emulsions; a comparison between constant pressure blocking laws and genetic programming (GP) model. *Desalination,* 329**,** 41-49.

GUTIG, C., GRADY, B. P. & STRIOLO, A. 2008. Experimental Studies on the Adsorption of Two SurfDFWDQWVRQ6ROLG$TXHRXV,QWHUIDFHV$VRUSWLRQ,VRWKHUPVDQG&DORULPHWULFV *Langmuir,* 24**,** 4806-4816.

HAIT, S. K., MAJHI, P. R., BLUME, A. & MOULIK, S. P. 2003. A Critical Assessment of Micellization of Sodium Dodecyl Benzene Sulfonate (SDBS) and Its Interaction with Poly(vinyl pyrrolidone) and Hydrophobically Modified Polymers, JR 400 and LM 200. *The Journal of Physical Chemistry B,* 107**,** 3650-3658.

IRITANI, E., KATAGIRI, N., ISHIKAWA, Y. & CAO, D.-Q. 2014. Cake formation and particle rejection in microfiltration of binary mixtures of particles with two different sizes. *Separation and Purification Technology,* 123**,** 214-220.

JAVADIAN, S. & KAKEMAM, J. 2017. Intermicellar interaction in surfactant solutions; a review study. *Journal of Molecular Liquids,* 242**,** 115-128.

JIMÉNEZ, S., MICÓ, M. M., ARNALDOS, M., MEDINA, F. & CONTRERAS, S. 2018. State of the art of produced water treatment. *Chemosphere,* 192**,** 186-208.

KOSMULSKI, M. 2006. pH-dependent surface charging and points of zero charge: III. Update. *Journal of Colloid and Interface Science,* 298**,** 730-741.

KOU, J. & XU, S. 2016. In situ kinetics and conformation studies of dodecylamine adsorption onto zinc sulfide using a quartz crystal microbalance with dissipation (QCM-D). *Colloids and Surfaces A: Physicochemical and Engineering Aspects,* 490**,** 110-120.

KWON, H. J., BRADFIELD, C. K., DODGE, B. T. & AGOKI, G. S. Study of Fluid and Mass Adsorption Model in the QCM-D Sensor for Characterization of Biomolecular Interaction. COMSOL Conference, 2009 Boston, USA. https://www.comsol.com/paper/study-of-fluid-and-mass-adsorption-model-in-the-qcm-d-sensor-for-characterizatio-6561: COMSOL.

LARGITTE, L. & PASQUIER, R. 2016. A review of the kinetics adsorption models and their application to the adsorption of lead by an activated carbon. *Chemical Engineering Research and Design,* 109**,** 495-504.

LIU, D., YAN, Y., LEE, K. & YU, J. 2009. Effect of surfactant on the alumina dispersion and corrosion behavior of electroless Ni-P-Al2O3 composite coatings. *Materials and Corrosion,* 60**,** 690-694.

LIU, S. X. & KIM, J.-T. 2009. Study of adsorption kinetics of surfactants onto polyethersulfone membrane surface using QCM-D. *Desalination,* 247**,** 355-361.

LU, D., ZHANG, T. & MA, J. 2015. Ceramic Membrane Fouling during Ultrafiltration of Oil/Water Emulsions: Roles Played by Stabilization Surfactants of Oil Droplets. *Environmental Science & Technology*.

LU, D., ZHANG, T., GUTIERREZ, L., MA, J. & CROUÉ, J.-P. 2016. Influence of Surface Properties of Filtration-Layer Metal Oxide on Ceramic Membrane Fouling during Ultrafiltration of Oil/Water Emulsion. *Environmental Science & Technology,* 50**,** 4668-4674.

0$2-/29,á7KH.UDIIWWHPSHUDWXUHRIVXUIDFWDQWVROXWLRQV *Thermal Science,* 16**,** 631-640.

MATOS, M., GUTIÉRREZ, G., LOBO, A., COCA, J., PAZOS, C. & BENITO, J. M. 2016. Surfactant effect on the ultrafiltration of oil-in-water emulsions using ceramic membranes. *Journal of Membrane Science,* 520**,** 749-759.

MOULIK, S. P., HAQUE, M. E., JANA, P. K. & DAS, A. R. 1996. Micellar Properties of Cationic Surfactants in Pure and Mixed States. *The Journal of Physical Chemistry,* 100**,** 701-708.

MROUE, K. H., EMWAS, A.-H. M. & POWER, W. P. 2010. Solid-state 27Al nuclear magnetic resonance investigation of three aluminum-centered dyes. *Canadian Journal of Chemistry,* 88**,** 111-123.

NGANG, H. P., AHMAD, A. L., LOW, S. C. & OOI, B. S. 2017. Adsorption-desorption study of oil emulsion towards thermo-responsive PVDF/SiO2-PNIPAM composite membrane. *Journal of Environmental Chemical Engineering,* 5**,** 4471-4482.

3,6Ëý0(9Ë6.<)383Ë0 5. Determination of micelle aggregation numbers of alkyltrimethylammonium bromide and sodium dodecyl sulfate surfactants using time-resolved fluorescence quenching. *Open Chemistry*.

REVIAKINE, I., JOHANNSMANN, D. & RICHTER, R. P. 2011. Hearing What You Cannot See and Visualizing What You Hear: Interpreting Quartz Crystal Microbalance Data from Solvated Interfaces. *Analytical Chemistry,* 83**,** 8838-8848.

SAAD ALAMI, Y., MAJDA, B. & BRAHIM, A. 2018. Alumina Membranes for Desalination and Water Treatment.

SEYED SHAHABADI, S. M. & REYHANI, A. 2014. Optimization of operating conditions in ultrafiltration process for produced water treatment via the full factorial design methodology. *Separation and Purification Technology,* 132**,** 50-61.

SILALAHI, S. H. D., LEIKNES, T., ALI, J. & SANDERSON, R. 2009. Ultrasonic time domain reflectometry for investigation of particle size effect in oil emulsion separation with crossflow microfiltration. *Desalination,* 236**,** 143-151.

SOOD, A. K. & AGGARWAL, M. 2018. Evaluation of micellar properties of sodium dodecylbenzene sulphonate in the presence of some salts. *Journal of Chemical Sciences,* 130.

TUMMONS, E. N., TARABARA, V. V., CHEW, JIA W. & FANE, A. G. 2016. Behavior of oil droplets at the membrane surface during crossflow microfiltration of oil–water emulsions. *Journal of Membrane Science,* 500**,** 211-224.

WESCHENFELDER, S. E., BORGES, C. P. & CAMPOS, J. C. 2015a. Oilfield produced water treatment by ceramic membranes: Bench and pilot scale evaluation. *Journal of Membrane Science,* 495**,** 242-251.

WESCHENFELDER, S. E., LOUVISSE, A. M. T., BORGES, C. P., MEABE, E., IZQUIERDO, J. & CAMPOS, J. C. 2015b. Evaluation of ceramic membranes for oilfield produced water treatment aiming reinjection in offshore units. *Journal of Petroleum Science and Engineering,* 131**,** 51-57.

WESCHENFELDER, S. E., MELLO, M. C. C., BORGES, C. P. & CAMPOS, J. C. 2015c. Oilfield produced water treatment by ceramic membranes: Preliminary process cost estimation. *Desalination,* 360**,** 81-86.

YUE, M. B., XUE, T., JIAO, W. Q., WANG, Y. M. & HE, M.-Y. 2011. CTAB-directed synthesis of PHVRSRURXV alumina promoted by hydroxy carboxylate: The interplay of tartrate and CTAB. *Solid State Sciences,* 13**,** 409-416.

Table 1. Kinetic parameters for SDBS adsorption on the three metal oxides (SDBS concentrations < CMC)

Metal oxide	k (cm^2/mM.ng.s)	k^{-1} (cm^2/ng.s)	k/k^{-1} (1/mM)
TiO_2	$2.0x10^{-3}$	$2.0x10^{-5}$	1000.0
ZrO_2	$1.3x10^{-3}$	$3.9x10^{-4}$	3.3
Al_2O_3	$2.7x10^{-4}$	$6.6x10^{-4}$	0.4

Table 2. Adsorption rate ($_2$) and adsorption capacity (qe) of 1 mM SDBS solution as a function of pH. $_2$ and qe obtained are expressed in cm^2/ng.s and ng/cm^2, respectively.

	pH	Surface charge	$_2$	qe
TiO_2 (pH_{pzc} 5.2-6.3)	3.0	+	3.3x10^{-4}	292.6
	6.8	-*	1.2x10^{-3}	12.0
	9.4	-	$2.1x10^{-3}$	11.7
ZrO_2 (pH_{pzc} 5.5-6.6)	3.0	+	$3.2x10^{-6}$	270.9
	6.8	-*	$1.6x10^{-3}$	24.9
	9.4	-	$1.4x10^{-3}$	18.2
Al_2O_3 (pH_{pzc} 7.4-8.6)	3.0	+	$2.5x10^{-4}$	191.1
	6.8	+*	$8.6x10^{-4}$	29.1
	9.4	-	$2.1x10^{-3}$	17.9

*Although charged at this pH, these surfaces are close to an overall neutral charge

Table 3. Kinetic parameters for CTAB concentrations lower than CMC

Metal oxide	k (cm^2/mM.ng.s)	k^{-1} (cm^2/ng.s)	k/k^{-1} (1/mM)
TiO_2	$2.9x10^{-5}$	$4.2x10^{-5}$	0.7
ZrO_2	$3.6x10^{-5}$	$2.6x10^{-6}$	13.8
Al_2O_3	-	-	-

Table 4. CTAB adsorption rates ($_2$) and adsorption capacity (qe) at different pH. $_2$ and qe obtained are expressed in cm^2/mM ng.s and ng/cm^2, respectively

Metal oxide	pH	Surface charge	$_2$	qe
TiO_2 (pH_{pzc} 5.2-6.3)	3.0	+	$6.38x10^{-5}$ [k]	324.9
	6.8	-[*]	$5.8x10^{-5}$	336.6
	9.4	-	$4.1x10^{-5}$	373.9
ZrO_2 (pH_{pzc} 5.5-6.6)	3.0	+	$1.2x10^{-4}$ [k]	236.4 [k]
	6.8	-[*]	$2.1x10^{-5}$	278.4
	9.4	-	$6.9x10^{-5}$	303.44
Al_2O_3 (pH_{pzc} 7.4-8.6)	3.0	+	$2.36x10^{-4}$ [k]	151.1 [k]
	6.8	-[*]	-	-
	9.4	-	$3.1x10^{-5}$	309.1

[*]Although charged at this pH, these surfaces are close to an overall neutral charge

[k] $_2$ and qe obtained from the first step reaction (rigid film in Figure 3d)